Cryostructure and Uniaxial Compressive Strength of Ice-Rich Permafrost in Northern Alaska

Ziyi Wang¹; Ming Xiao²; and Matthew Bray³

¹Dept. of Civil and Environmental Engineering, Pennsylvania State Univ., University Park, PA. Email: ziyiwang@psu.edu

²Dept. of Civil and Environmental Engineering, Pennsylvania State Univ., University Park, PA. Email: mzx102@psu.edu

³Institute of Northern Engineering, Univ. of Alaska Fairbanks, Fairbanks, AK.

Email: mtbray@alaska.edu

ABSTRACT

Knowledge of ground ice type and volume in the upper permafrost are vital for engineering design in cold regions. Cryostructure, which describes the pattern of ice inclusions, is an indicator of the formation characteristics and geology of permafrost soil and affects the geomechanical behavior of permafrost. In this paper, we present field sampling of relatively undisturbed permafrost on the Arctic Coastal Plain near Utqiagvik, Alaska. We characterize the cryostructure of the permafrost samples that were retrieved from five boreholes, which primarily consisted of organic silty sand with suspended ice inclusions. We conducted a series of unconfined compression tests under constant strain rate at temperatures of -2°C and -10°C to investigate the geomechanical behavior of selected permafrost cores. Here, we present the effects of temperature, dry density, water content, and cryostructure on the geomechanical behavior of ice-rich permafrost. Considering the effect of temperature, an empirical equation for short-term peak compressive strength is developed based on the experimental results. A quantitative example is provided to demonstrate how the varying geomechanical properties affect ultimate bearing capacity of shallow foundations in permafrost.

Keywords: permafrost, ground ice, cryostructure, geomechanical behavior, foundation, Alaska

INTRODUCTION

Permafrost is widely distributed in the high latitude regions and occupies 24% of the land area of the northern hemisphere (Anisimov & Nelson 1996). The top layer above the permafrost, which freezes in the winter and thaws in the summer, is the active layer. In the Arctic, permafrost has served as a strong foundation for civil infrastructure. Since the average active layer thickness (ALT) in the Arctic region is less than 1 m, foundations can be anchored into the permafrost to provide adequate support for superstructures to resist various loads (Nixon & McRoberts 1976). Global climate change, however, is driving the warming of the Arctic at up to four times the rate of lower latitudes (Rantanen et al. 2022). As air temperatures in the Arctic increase over time, ground temperatures rise, driving near-surface permafrost degradation (Biskaborn et al. 2019). Various modes of permafrost degradation, including ground subsidence, active layer thickening, and talik formation, could affect foundation performance, inducing irreversible damage to Arctic civil infrastructure (Andersland & Ladanyi 2003; Clarke 2007; Hjort et al. 2022; Wang et al. 2023a, b). The cumulative costs of climate-related damage to Alaskan infrastructure were

estimated to be \$5.5 billion for Representative Concentration Pathway (RCP) 8.5 and \$4.2 billion for RCP 4.5 from 2015 to 2099 (Melvin et al. 2017). Understanding how permafrost resists failure and deformation under complex thermal-hydro-mechanical conditions is essential to quantify the stability of civil infrastructure foundations (Thomas et al. 2009).

Cryogenic structure or cryostructure is the pattern of ice inclusions within a frozen soil (Bray et al. 2012). The pattern of ice inclusion is closely associated with cryolithology and Quaternary depositional environments. Thus, cryostructure serves as a direct indicator of the geology of permafrost. The type of cryostructure controls the geophysical and geomechanical characteristics of permafrost including ice content, unfrozen water content, thermal conductivity, thaw settlement, and creep. Given the importance of these characteristics, the characterization of cryostructure becomes crucial for foundation design in cold regions.

The degradation of permafrost deteriorates the geomechanical properties of frozen soils (Razbegin et al. 1996), such as the stress-strain response, elastic and dynamic properties, strength and stiffness parameters (Liew et al. 2022). Most of the experiments reported in the literature have been conducted on remolded, reconstituted, or artificially-frozen soil specimens. The mechanical behavior of remolded and undisturbed samples can exhibit significant disparities even with a similar ice content, primarily due to variations in cryostructure. Given the scarcity of known *in situ* permafrost properties and the significance of these properties in designing resilient civil infrastructure, it is important to collect undisturbed permafrost samples and investigate their geophysical and geomechanical properties for foundation design in Northern Alaska.

The main objective of this study is to characterize the cryostructure and geomechanical behavior of ice-rich permafrost for foundation design in northern Alaska. This paper first presents the description of cryostructure of permafrost samples retrieved from five boreholes on the tundra near Utqiagvik, Alaska. Index properties – water content, dry density, frozen wet density, specific gravity, Atterberg limits, and particle size distribution – are determined to characterize the representative permafrost samples. Second, unconfined compression tests are conducted on representative samples at temperatures of -2°C and -10°C. The strength and stiffness of permafrost are determined, including ultimate compressive strength, yield strength, and elastic modulus. Third, an empirical equation is established based on experimental results, which determine short-term peak compressive strength at different temperatures. A quantitative example is provided to demonstrate how the varying geomechanical properties affect ultimate bearing capacity of shallow foundations in permafrost.

STUDY SITE, GEOLOGICAL HISTORY, AND SOIL SAMPLING

The field sampling was conducted at five locations on the tundra near Utqiagvik, Alaska in August 2022. Figure 1 presents an aerial view of the tundra with the layouts of the five boreholes, labeled S1 (71.3231°N 156.6144°W), S2 (71.3244°N 156.6103°W), S3 (71.3264°N 156.5994°W), S4 (71.3294°N 156.5933°W), and S5 (71.3322°N 156.5842°W). A total of 562.1 cm of relatively undisturbed permafrost cores of 4.0 – 4.3 cm in diameter were obtained using a battery-powered auger. The active layer thickness of the permafrost tundra was in the range of 14 to 27.9 cm at the time of the sampling. The vegetated active layer was carefully removed at the borehole locations and set aside. Each permafrost core was wrapped in plastic wrap, covered with aluminum foil, and placed into a portable freezer with frozen gel packs to keep the sample

frozen. All collected cores were kept at negative temperatures during the whole period of transportation to the lab. After coring, the vegetated active layer was carefully restored to its original position.

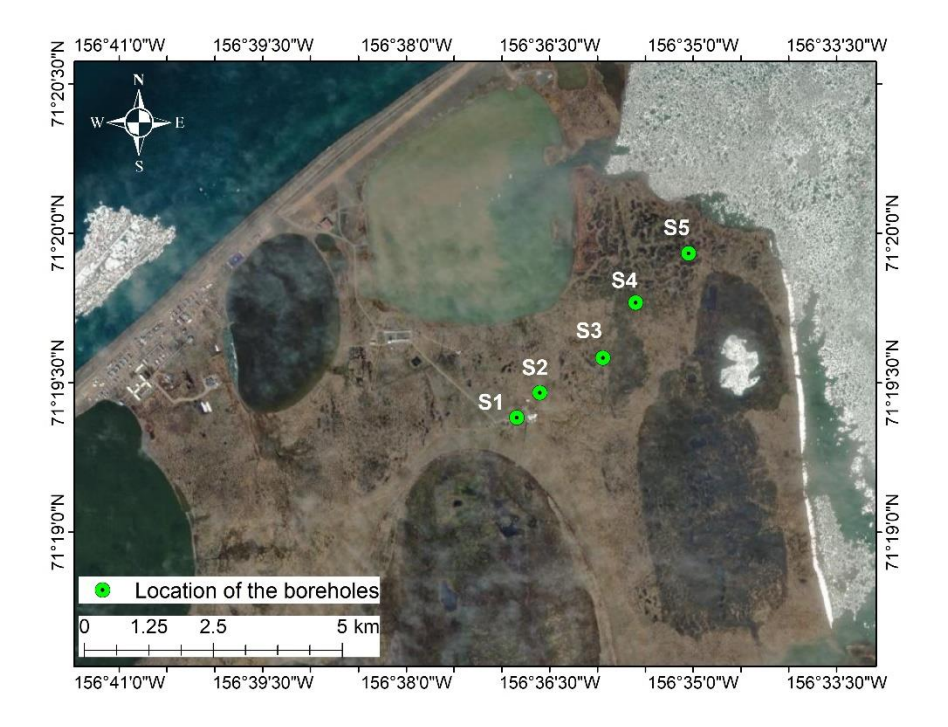


Figure 1. Aerial views of the five permafrost sampling locations in the tundra near Utqiagʻvik, AK (base map data from imagery copyright 2022 Maxar).

The study sites are located within the Barrow quadrangle of the geological map of Alaska (Wilson et al. 2015). This region is primarily covered with Quaternary unconsolidated surficial deposits, consisting mainly of silty and organic-rich sand.

Figure 2 depicts the cryostratigraphy within the primary surficial deposits at the study sites. At location S1 (Figure 2a), the active layer thickness was 14 cm during sampling time. From 14 to 90 cm depth, the core was primarily dark brown clayey silt with gravel. Ice occurred occasionally as 1.3-cm thick lenticular ice lenses. From 90 to 103 cm, the soil was medium brown organic silty sand with sparse fine gravel and reticulate ice.

At location S2 (Figure 2b), the active layer thickness was 21.6 cm during sampling. The soil consisted of peat with woody fragments and roots from 21.6 to 36.8 cm. Ice was present as thin lenticular lenses and random ice lenses up to 1-mm thick. From 36.8 to 83.8 cm, the core segments were primarily ice containing horizontal organic inclusions up to 1-cm thick. The lower portion of this zone contained vertical organic inclusions. From 83.8 to 147 cm, a general transition was observed from gray ice-rich slightly organic sand to medium brown slightly sandy organic silt with sparse fine gravel intermixed with ice zones. From 152 to 170 cm, the soil was brown silty sand with sparse fine gravel and contained only pore ice with minimal organic content, which was a notable shift from the overlying soil sequences with higher organic content. The organic content decreased with depth.

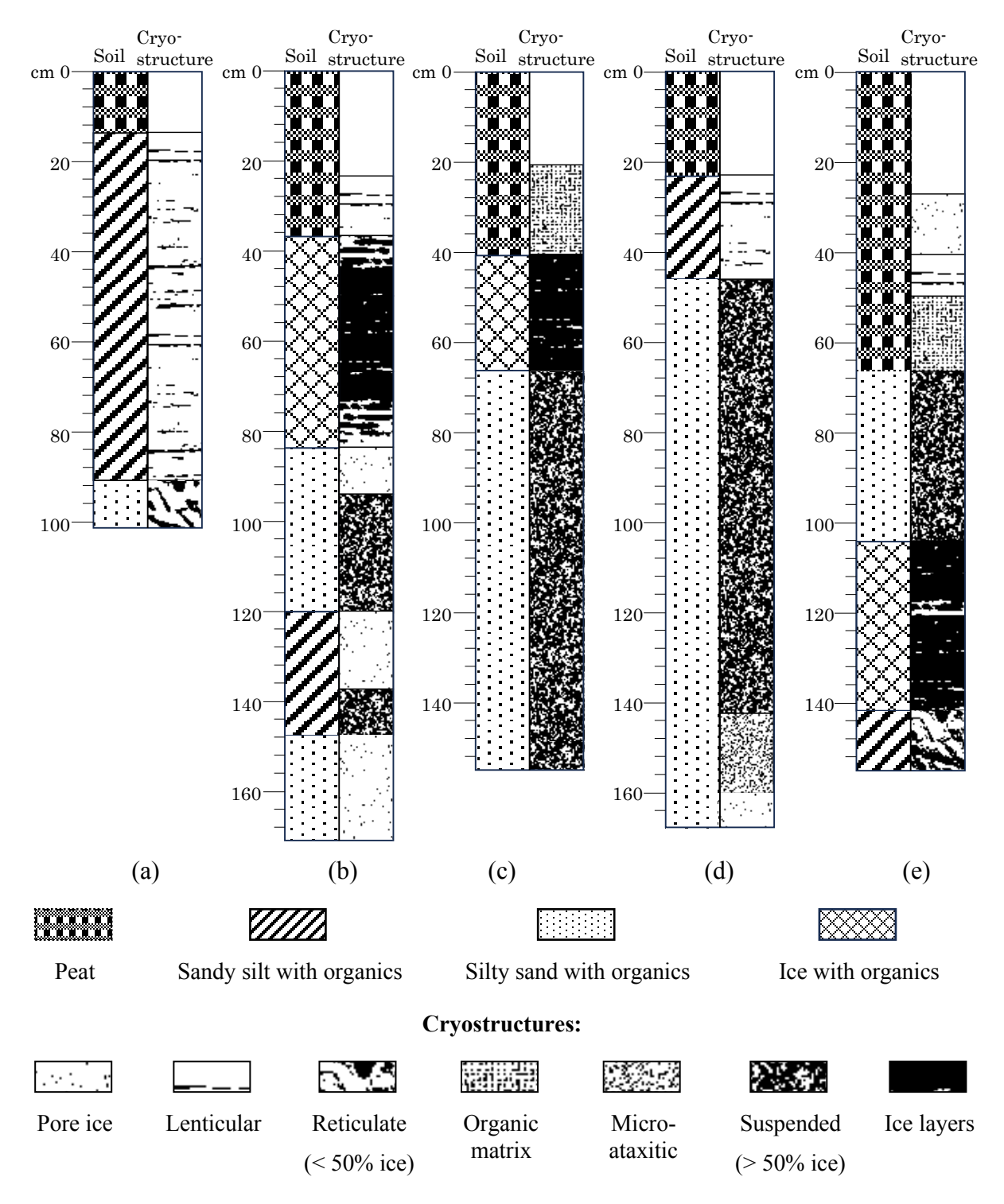


Figure 2. Cryostratigraphy of Arctic coastal plain deposits at the five sampling locations: (a) location S1; (b) location S2; (c) location S3; (d) location S4; and (e) location S5. The cryostructure classification system is modified based on Kanevskiy et al. (2013)

At location S3 (Figure 2c), the active layer thickness was 20.3 cm. The soil was ice-rich, and composed primarily of peat, organic silt, and silty sand. The sand was highly silty with sparse

fine gravel. From 20.3 to 40.6 cm, the soil was peat to silty peat. Ice was present in an organic matrix above 30.5 cm; below 30.5 cm were organics suspended in ice. From 40.6 to 66.0 cm, the soil was primarily ice with thin suspended organics. Below the ice layer, the soil was typically silty sand suspended within ice (i.e., ataxitic cryostructure). From 66.0 to 104.1 cm, the soil was medium brown organic silty sand. Below 104.1 cm, the soil was gray silty sand with minor organics.

At location S4 (Figure 2d), the active layer thickness was 23.8 cm during sampling. Most of the sampled sections were ice-rich. The soil consisted of silty peat to organic silt from 23.8 to 45.7 cm; organic silty sand suspended within ice from 48.3 to 142.2 cm; and silty sand with fine gravel with decreasing ice content with depth from 132.1 cm.

At location S5 (Figure 2e), the active layer thickness was 27.9 cm. The soil was peat to silty peat from 27.9 to 50.8 cm with pore ice (above 41.9 cm) and visible vertical and horizontal ice lenses (below 41.9 cm). From 50.8 to 64.8 cm, the soil was intermixed peat and medium brown organic soil. Ice was present in the organic matrix. From 64.8 to 104.1 cm, the soil consisted of intermixed peat and medium brown silty sand suspended in ice (i.e., ataxitic cryostructure). Ice with organic and silt layers occurred from 104.1 to 140.7 cm. From 140.7 to 154.9 cm, the soil was medium brown organic silt with layered and reticulate ice lenses up to 3-mm thick, with several ice lenses up to 2-cm thick.

GEOTECHNICAL PROPERTIES OF PERMAFROST PROPERTIES OF PERMAFROST SAMPLES

We tested six samples for unconfined compressive strength (UCS): three samples each at -2° C and -10° C. Figure 3 contains photographs of the permafrost samples before the UCS tests. Table 1 is a summary of the index properties of the six samples. The UCS tests were performed by the UAF Frozen Soil Testing (FROST) laboratory. The tests were performed on electromechanical screw-driven load frames, at a strain rate of 1% per minute according to ASTM D7300. The loading frames were placed in a walk-in cold room maintained at -5° C. Insulated chambers surrounded the loading pistons and frame. Within each chamber, a convection driven heat exchanger was placed in series with an external cold bath to achieve a specific temperature and maintain chamber temperature stability of $\pm 0.03^{\circ}$ C. The air temperature around the samples was monitored by four calibrated thermistors in close proximity to the sample. A latex membrane was placed around each sample to eliminate sublimation.

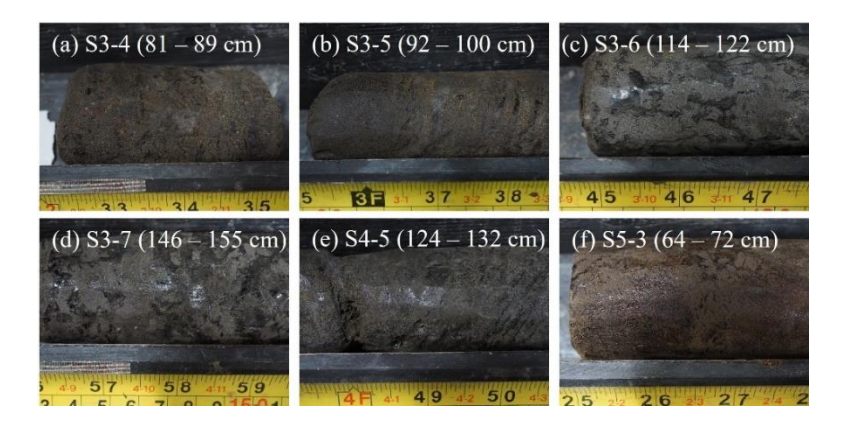


Figure 3. Selected permafrost cores for UCS testing.

Table 1. Summary of index properties of tested samples; ρ_{bf} is bulk frozen density, ρ_{dry} is dry density, w is gravimetric water content, θ_i is volumetric ice content, θ_w is volumetric water content, LL is liquid limit, PI is plasticity index, G_s is specific gravity.

-	D 41-				0	0			
Sample No.	Depth	$ ho_{bf}$	$ ho_{dry}$	W	θ_i	θ_w	- LL	PI	G_s
	(cm)	(g/cm^3)	(g/cm^3)	(%)	(%)	(%)			
S3-4	81-89	1.45	0.91	59.0	58.7	56.6	26	2	2.21
S3-5	92-100	1.57	1.05	50.1	57.2	55.0	26	1	2.44
S3-6	114-122	1.38	0.73	89.5	71.1	69.3	20	1	2.52
S3-7	146-155	1.23	0.49	149.7	80.4	79.0	22	1	2.52
S4-5	124-132	1.26	0.52	143.2	80.9	79.6	33	4	2.72
S5-3	64-72	1.05	0.27	295.9	85.6	84.5	27	3	1.84

The grain size distributions (GSD) of the samples used for the UCS tests were determined by conducting sieve analysis and hydrometer analysis, as per ASTM C136 and ASTM D422, respectively. Figure 4 contains the GSD of the selected samples, which are classified as organic ice-rich silty sand (SM).

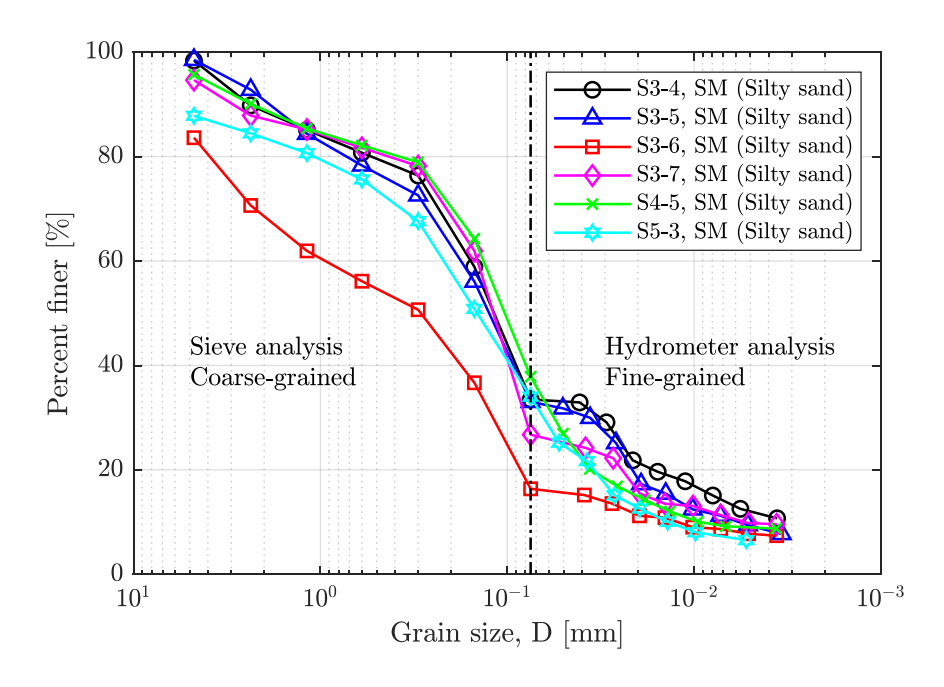


Figure 4. Grain size distributions of selected samples.

RESULTS

Figure 5 contains photographs of permafrost samples after UCS testing. For samples S3-4, S3-6, S3-7, we observed prevalent external shear and tensile cracks. Samples S3-4 and S3-5 exhibited significant external cracks and dilation after compression. Sample S4-5, a silty sand of the finest GSD among the six samples, developed a clear shear zone. Sample S5-3 displayed a localized shear zone with intense cracking and dilation in two sections with high ice content.

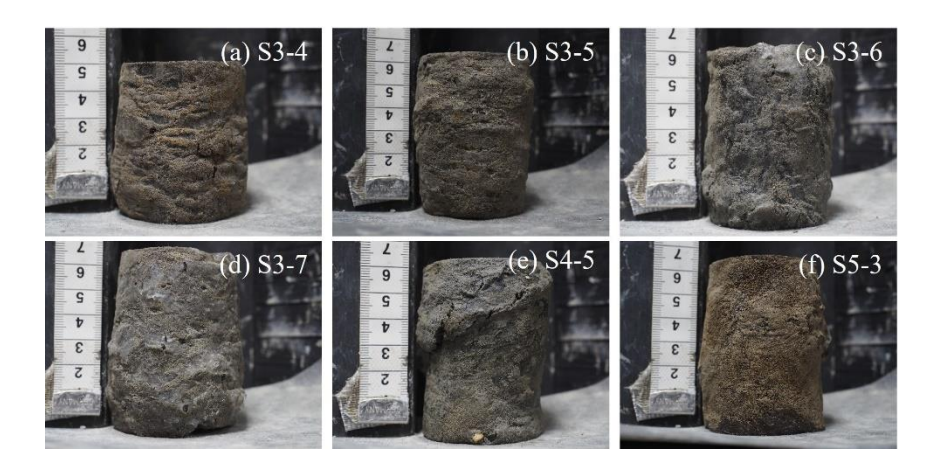


Figure 5. Deformation of permafrost samples after UCS tests.

Figure 6 depicts the relationship between stress and strain of six permafrost samples during UCS testing. Figures 6a and 6b present the stress-strain responses of the samples at -2°C and -10°C, respectively. The dry densities of the samples are listed in Figure 6 and range from 270 to 1050 kg/m³. As the temperature decreases, the peak compressive strength σ_m increases. The samples with higher ice content and lower dry density behave as brittle material with a failure strain of about 1% soon after plastic yielding. The soil becomes ductile at higher dry density and lower ice content, where there is no significant difference between yield strength and peak strength resulting from strain hardening. Our results are consistent with those of Zhu & Carbee (1984). The reason for the difference is that the ice matrix of denser soil facilitates enhanced frictional interaction among soil particles.

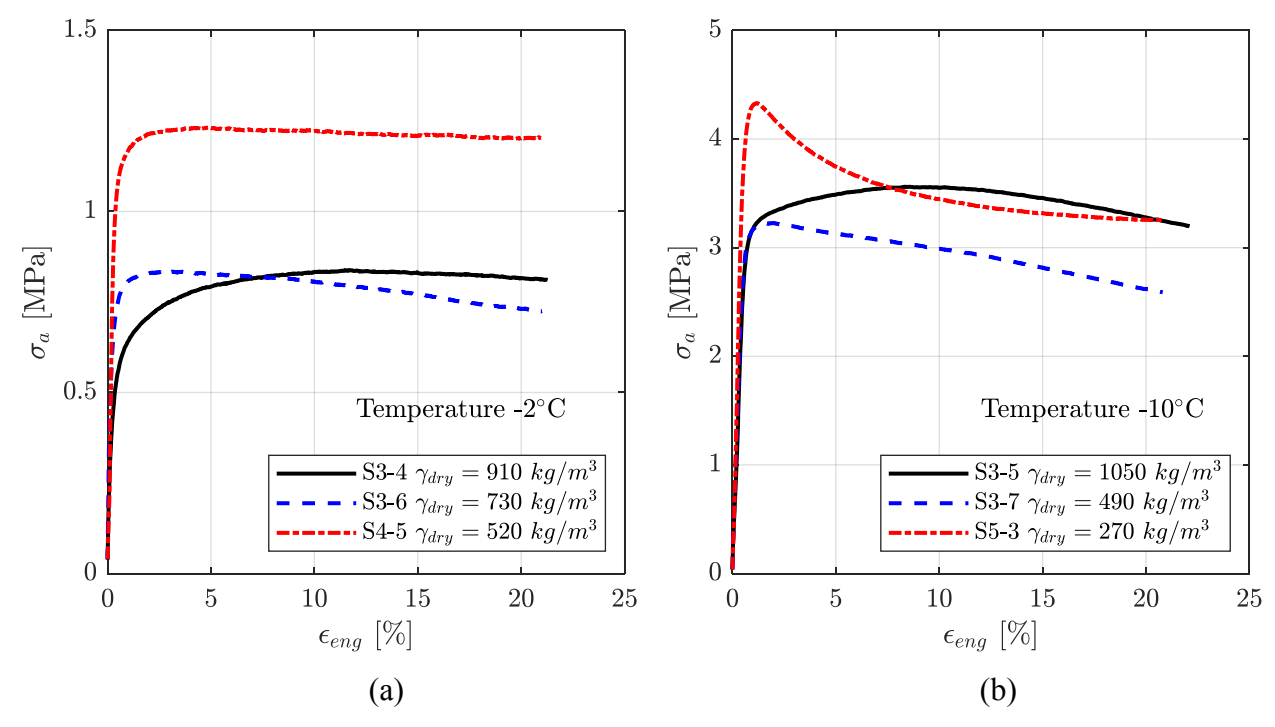


Figure 6. Stress-strain response of permafrost samples during UCS tests: (a) axial stress versus axial strain at -2°C; (b) axial stress versus axial strain at -10°C.

ANALYSIS AND DISCUSSIONS

Figure 7 is a plot of $\log \sigma_m$ versus $\log (T/T_0)$ for ice-rich silty sand with organics, where σ_m is the peak strength of frozen soil in MPa, T_0 is the reference temperature of -1 °C, and T is temperature. The triangle and square data points are from previous studies on organic ice-rich silty permafrost (Yang et al. 2015) and on remolded frozen silt (Zhu & Carbee 1984), respectively. Our test data indicates that the peak strength of frozen silty sand significantly increases with decreasing temperature. Two data points at -2°C from this study overlap with approximately the same peak compressive strength. The peak strength of frozen soil as a function of temperature can be written as (Sayles & Haines 1974):

$$\sigma_m = A \left(\frac{T}{T_0}\right)^m \tag{1}$$

where A is an empirical parameter with the dimension of stress, and m is a dimensionless parameter.

Based on our regression analysis, the values of A and m are 0.5430 and 0.8341, respectively. The fitting curve in this study is steeper compared with the previous regression curves by Zhu & Carbee (1984) and Yang et al. (2015). At warmer sub-freezing temperatures, the short-term peak strength presented here is lower compared to that from prior research. This may be attributed to the ice-rich nature of the tested samples and their non-uniform distribution of ice. The ice contributes to the yield behavior and influences the peak strength behavior of ice-rich permafrost.

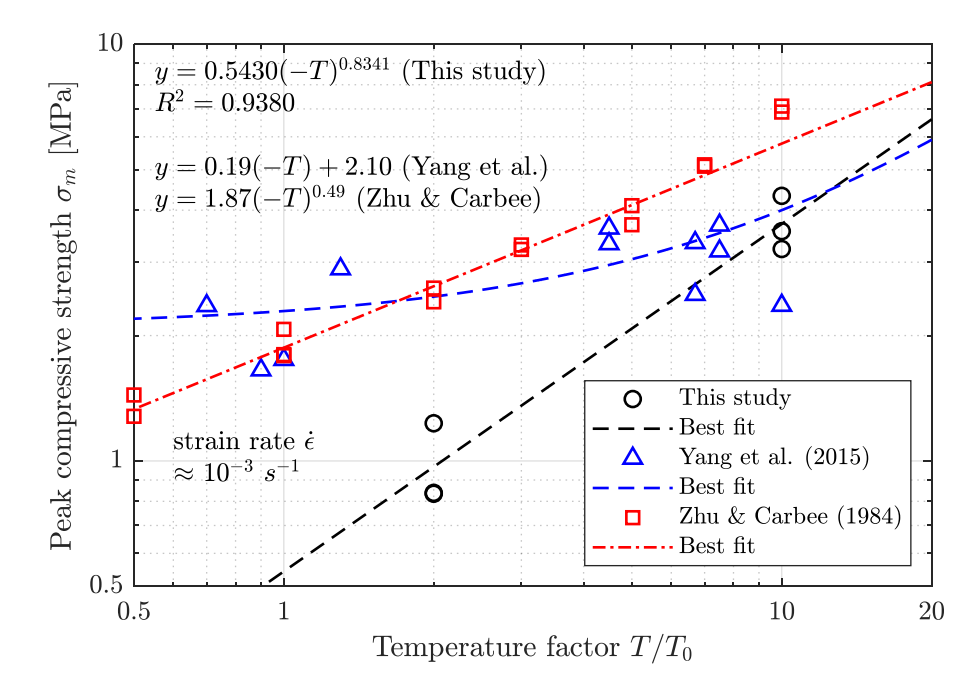


Figure 7. Plot of $\log \sigma_m$ versus $\log (T/T_\theta)$ for ice-rich silty soil with organics, including a comparison with previous studies. T_θ is the reference temperature of -1 °C.

Figure 8 is a schematic of a typical shallow foundation in permafrost. A low adhesion layer is placed around the footing in the active layer to minimize the frost heave forces acting on the foundation. An insulated floor and beam, and an air space between the ground and the floor are used to reduce heat transfer between the soil and the floor and beam. The embedment depth of the footing is D_f and the width of the footing is B.

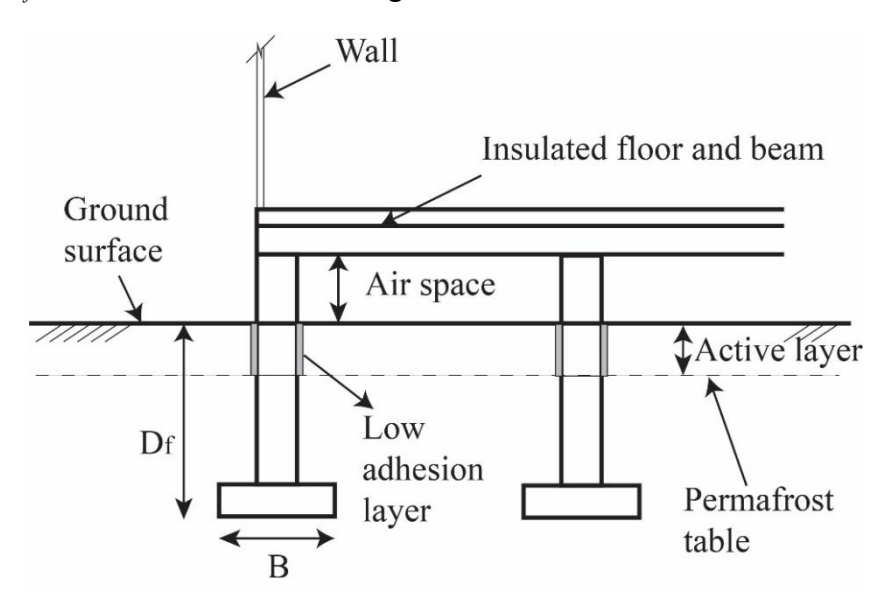


Figure 8. A schematic of a typical shallow foundation footing in permafrost.

As illustrated in Figure 5, plastic failure with localized strain (i.e., shear band) was observed during UCS testing. This plastic failure mode of permafrost allows us to use Terzaghi's theory to calculate the short-term bearing capacity. In this study, we use the general bearing capacity theory to calculate the shore-term ultimate bearing capacity. Considering vertical loads and rigid-plastic soil behavior, the calculation of short-term ultimate bearing capacity of a shallow foundation is (Meyerhof 1963):

$$q_{ult} = c' N_c F_{cs} F_{cd} + q N_q F_{qs} F_{qd} + 0.5 \gamma B N_{\gamma} F_{\gamma s} F_{\gamma d}$$
 (2)

where c' is the short-term cohesion, q is the soil surcharge, γ is the unit weight of soil, B is the width of shallow foundation. N_c , N_q , and N_γ are the bearing capacity factors. For frictionless ice-rich frozen soil they are:

$$N_q = 1$$

$$N_c = \pi + 2 = 5.14$$

$$N_{\gamma} = 0$$
(3)

 F_{cs} , F_{qs} , and $F_{\gamma s}$ are the shape factors; for frictionless soil they are:

$$F_{cs} = 1 + 0.2 \tan^2(45 + \frac{\phi'}{2}) \frac{B}{L} = 1 + 0.2 \frac{B}{L}$$

$$F_{qs} = F_{\gamma s} = 1$$
(4)

 F_{cd} , F_{qd} , and $F_{\gamma d}$ are the depth factors; for frictionless soil they are:

$$F_{cd} = 1 + 0.2 \sqrt{\tan^2(45 + \frac{\phi'}{2})} \frac{D_f}{B} = 1 + 0.2 \frac{D_f}{B}$$

$$F_{qd} = F_{\gamma d} = 1$$
(5)

Combining these values produces Eq. 6, which is the calculation of short-term ultimate bearing capacity of a shallow foundation in frictionless ice-rich silty soil:

$$q_{ult} = 5.14c'(1 + 0.2\frac{B}{L})(1 + 0.2\frac{D_f}{B}) + q$$
 (6)

Considering the effect of active layer thickness, Eq. 7 is the calculation of soil surcharge at the bottom of the footing, q:

$$q = \gamma_{ba}D_a + \gamma_{bp}D_p = \gamma_{ba}D_a + \gamma_{bp}(D_f - D_a) \tag{7}$$

where D_a is the active layer thickness, D_p is the embedment of the foundation in permafrost, γ_{ba} is the bulk unit weight of active layer, and γ_{bp} is the bulk unit weight of permafrost. For frictionless frozen soil, the short-term cohesion can be defined by:

$$c' = \frac{\sigma_m(T)}{2} \tag{8}$$

where $\sigma_m(T)$ is the temperature-dependent, short-term peak compressive strength determined from UCS testing. For ice-rich organic silty soil, Eq. 1 with the constants determined from this research can be used to calculate σ_m at different temperatures:

$$\sigma_m(T) = A \left(\frac{T}{T_0}\right)^m = 0.5430(-T)^{0.8341} \times 10^3 [kPa]$$
 (9)

The bearing capacity equation for ice-rich organic silty sand can be re-written as follows:

$$q_{ult} = 5.14 \times \frac{A}{2} \times 10^{3} (-T)^{m} \left(1 + 0.2 \times \frac{B}{L} \right) \left(1 + 0.2 \times \frac{D_{f}}{B} \right) + \gamma_{ba} D_{a} + \gamma_{bp} (D_{f} - D_{a})$$
(10)

These equations are demonstrated using a numeric example. We consider a typical shallow foundation in permafrost as presented in Figure 8. We use the following parameters in the design of the shallow foundation: 1) active layer thickness, D_a , is 0.3 m; 2) embedment of foundation in permafrost, D_p , is at least 2 times of D_a to resist frost heaving; 3) total embedment depth, D_f , equals to the summation of D_a and D_p , which is at least 0.9 m; 4) a square footing with width B_a and length D_a of 1.0 m; 5) assume a homogeneous subsurface with frozen bulk density of permafrost, ρ_{bp} , of 1320 kg/m³ and bulk density of the active layer, ρ_{ba} , of 1960 kg/m³.

Figure 9 illustrates the variation of short-term ultimate bearing capacity of a square footing in ice-rich organic silty sand with temperature considering different embedment depths. The ultimate bearing capacity increases with the decrease of temperature and increase of embedment depth. When the ground temperature increases from -10 °C to -2 °C, the short-term ultimate bearing capacity reduces by 73.8% for the embedment of 1.5 m considered in Figure 9.

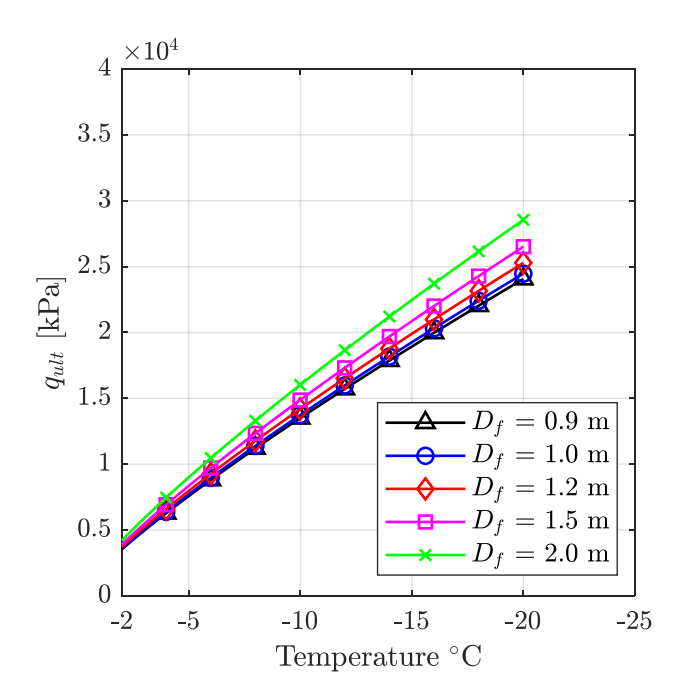


Figure 9. Variation of short-term ultimate bearing capacity with temperature considering different embedment depths D_f .

CONCLUSIONS

A geotechnical investigation on near-surface permafrost soils (upper 2m) sampled near Utqiagvik, Alaska was carried out for basic geotechnical characterization and short-term ultimate bearing capacity assessment. The permafrost soils are predominantly organic and icerich with ataxitic cryostructure (i.e., soil suspended in ice). The soils selected for mechanical testing are classified as silty sand. An empirical equation to determine peak compressive strength of ice-rich organic silty sand is developed based on the UCS testing results. Using the empirical equation for peak compressive strength, a short-term ultimate bearing capacity equation is established. Using the equation, an example quantitatively shows that permafrost warming significantly affects a shallow foundation's bearing capacity.

ACKNOWLEDGEMENTS

This study was supported by the U.S. National Science Foundation under Grant Numbers: ICER-1927718 and CMMI- 2034363. Dr. Margaret Darrow at the University of Alaska Fairbanks coordinated the lab testing, participated in the data analysis, and reviewed the manuscript.

REFERENCES

- Andersland, O.B. and Ladanyi, B., 2003. *Frozen ground engineering*. John Wiley & Sons. Anisimov, O.A. and Nelson, F.E., 1996. Permafrost distribution in the Northern Hemisphere under scenarios of climatic change. *Global and Planetary Change*, 14(1-2), pp.59-72.
- ASTM Int'l, 2006. Standard Test Method for Laboratory Determination of Strength Properties of Frozen Soil at a Constant Rate of Strain. D 7300 06.
- ASTM Int'l, 2006. Standard Test Method for Sieve Analysis of Fine and Coarse Aggregates, C 136.
- ASTM Int'l, 2007. Standard Test Method for Particle-Size Analysis of Soils, D 422 63.
- Biskaborn, B.K., Smith, S.L., Noetzli, J., Matthes, H., Vieira, G., Streletskiy, D.A., Schoeneich, P., Romanovsky, V.E., Lewkowicz, A.G., Abramov, A. and Allard, M., 2019. Permafrost is warming at a global scale. *Nature communications*, 10(1), p.264.
- Bray, M.T., 2012. The influence of cryostructure on the creep behavior of ice-rich permafrost. *Cold regions science and technology*, 79, pp.43-52.
- Clarke, E.S. ed., 2007, September. Permafrost foundation: state of the practice. American Society of Civil Engineers.
- Hjort, J., Streletskiy, D., Doré, G., Wu, Q., Bjella, K. and Luoto, M., 2022. Impacts of permafrost degradation on infrastructure. *Nature Reviews Earth & Environment*, 3(1), pp.24-38.
- Hults, C.P., Mull, C.G. and Karl, S.M., 2015. *Geologic map of Alaska*. US Department of the Interior, US Geological Survey.
- Kanevskiy, M., Shur, Y., Jorgenson, M.T., Ping, C.L., Michaelson, G.J., Fortier, D., Stephani, E., Dillon, M. and Tumskoy, V., 2013. Ground ice in the upper permafrost of the Beaufort Sea coast of Alaska. *Cold Regions Science and Technology*, 85, pp.56-70.
- Liew, M., Ji, X., Xiao, M., Farquharson, L., Nicolsky, D., Romanovsky, V., Bray, M., Zhang, X. and McComb, C., 2022. Synthesis of physical processes of permafrost degradation and geophysical and geomechanical properties of permafrost. *Cold Regions Science and Technology*, 198, p.103522.
- Melvin, A.M., Larsen, P., Boehlert, B., Neumann, J.E., Chinowsky, P., Espinet, X., Martinich, J., Baumann, M.S., Rennels, L., Bothner, A. and Nicolsky, D.J., 2017. Climate change damages to Alaska public infrastructure and the economics of proactive adaptation. *Proceedings of the National Academy of Sciences*, 114(2), pp.E122-E131.
- Meyerhof, G.G., 1963. Some recent research on the bearing capacity of foundations. *Canadian geotechnical journal*, 1(1), pp.16-26.
- Nixon, J.F. and McRoberts, E.C., 1976. A design approach for pile foundations in permafrost. *Canadian Geotechnical Journal*, 13(1), pp.40-57.
- Rantanen, M., Karpechko, A.Y., Lipponen, A., Nordling, K., Hyvärinen, O., Ruosteenoja, K., Vihma, T. and Laaksonen, A., 2022. The Arctic has warmed nearly four times faster than the globe since 1979. *Communications Earth & Environment*, 3(1), p.168.
- Razbegin, V.N., Vyalov, S.S., Maksimyak, R.V. and Sadovskii, A.V., 1996. Mechanical properties of frozen soils. *Soil mechanics and foundation engineering*, 33(2), pp.35-45.
- Sayles, F.H. and Haines, D., 1974. Creep of frozen silt and clay (No. 252). Corps of Engineers, US Army, Cold Regions Research and Engineering Laboratory.

- Thomas, H.R., Cleall, P., Li, Y.C., Harris, C. and Kern-Luetschg, M., 2009. Modelling of cryogenic processes in permafrost and seasonally frozen soils. *Geotechnique*, 59(3), pp.173-184.
- Wang, Z., Xiao, M., Liew, M., Jensen, A., Farquharson, L., Romanovsky, V., Nicolsky, D., McComb, C., Jones, B.M., Zhang, X. and Alessa, L., 2023a. Arctic geohazard mapping tools for civil infrastructure planning: a systematic review. *Cold Regions Science and Technology*, p.103969.
- Wang, Z., Xiao, M., Nicolsky, D., Romanovsky, V., McComb, C. and Farquharson, L., 2023b. Arctic coastal hazard assessment considering permafrost thaw subsidence, coastal erosion, and flooding. *Environmental Research Letters*, 18(10), p.104003.
- Yang, Z.J., Still, B. and Ge, X., 2015. Mechanical properties of seasonally frozen and permafrost soils at high strain rate. *Cold regions science and technology*, 113, pp.12-19.
- Zhu, Y. and Carbee, D.L., 1984. Uniaxial compressive strength of frozen silt under constant deformation rates. *Cold regions science and technology*, 9(1), pp.3-15.